AIChE WILEY InterScience DISCOVER SOMETHING GREAT

Design and Optimization of Swirl Pipe Geometry for Particle-Laden Liquids

C. Ariyaratne
School of Engineering and Physical Sciences, University of Aberdeen, Aberdeen AB24 3UE, U.K

T. F. Jones
Institute of Particle Science and Engineering, University of Leeds, Leeds LS2 9JT, U.K

DOI 10.1002/aic.11122
Published online February 16, 2007 in Wiley InterScience (www.interscience.wiley.com).

A new generation of swirl-inducing pipes with continuously varying cross-sectional geometry have been designed with surprisingly beneficial results. The advantages of swirl induction in pipes, particularly for improved transportation of particle-bearing liquids, are established. Coarse particles in water do not generally form stable suspensions and are of especial concern for a number of industrial processes. Swirling flow results in better particle distribution, requires low flow velocities to keep particles in suspension, and helps prevent pipeline blockage. Improved wear performance can be inferred from greater numbers of particles supported by the flow, and reduced impact angles and impact velocities. Historically, research into swirl-inducing pipes has indicated a lobed helical geometry of fixed cross section and constant helix as the near optimum design in swirl induction, at a low pressure cost. In addition to its hydraulic advantages, the lobed design dredges particles into the flow in a smooth mechanical action. Transition ducts to such swirl pipes were designed for the primary purpose of reducing entry and exit pressure losses. However, increased exit swirl intensities and reduced rate of swirl decay indicate swirl pipes with continuously varying cross-sectional geometry are the way forward. © 2007 American Institute of Chemical Engineers *AIChE J,* 53: 757–768, 2007

Keywords: pipe design, hydraulic transport, swirl, computational fluid dynamics (CFD), particle-laden flow

Introduction

Hydraulic transport of solids has many advantages, such as its comparatively low environmental impact, its requirement for relatively little infrastructure, and the possibility of low operation and maintenance costs. It is crucial to the chemical, mining, and minerals industries. Swirling flow has the potential to improve important factors underlying the usefulness of hydraulic transport, such as pumping costs, erosion, pipeline blockage, and particle distribution.[1–10]

Previous researchers[1,11] used Fluent computational fluid dynamics (CFD) software in optimizing swirl pipe geometry. In a 0.05 m main, a four-lobed swirl pipe with an *equivalent diameter* of 0.05 m, length 0.4 m, and a *pitch*-to-diameter ratio 8:1, as illustrated in Figure 1, was most effective at swirl induction. The equivalent diameter is defined as the diameter of a circular pipe delivering fluid

Research carried out at School of Chemical Environmental and Mining Engineering, University of Nottingham, Nottingham NG7 2RD, U.K.
Correspondence concerning this article should be addressed to C. Ariyaratne at c.ariyaratne@abdn.ac.uk

© 2007 American Institute of Chemical Engineers

Figure 1. Optimized swirl pipe geometry as determined by previous researchers.

to the swirl pipe and of equal cross-sectional flow area to the lobed swirl pipe for continuity of flow.[1,2] The pitch is defined as the length for the pipe cross section to rotate by 360°.[3]

The optimization was carried out on the basis of *swirl effectiveness*, which is the ratio of *swirl intensity* generated to the normalized pressure loss across the pipe, where swirl intensity (S) is the ratio of the angular momentum flux to the product of the pipe radius and the axial momentum flux.[12,13]

$$S = \frac{\int_0^R uwr^2\, dr}{R\int_0^R u^2\, r\, dr} \tag{1}$$

$$\text{Swirl effectiveness} = \frac{S}{\left(\frac{\Delta P}{\frac{1}{2}\rho u^2}\right)} \tag{2}$$

The sudden change in cross section when flow transmits from circular pipe to lobed pipe results in high pressure losses. This can be avoided by providing a smooth transition zone, whereby the circular cross section gradually transforms to a lobed cross section and vice versa, as shown in Figure 2, at the entry and exit of a constant geometry swirl pipe.

The design of several different variable geometries based on the previously determined optimized constant geometry swirl pipe[14] was undertaken. These new designs were then optimized using CFD, based on the criterion of swirl effectiveness for use as entry and exit transition zones. In all cases, the optimization was based on indivisible *increments of twist*, where one increment of twist represents the axial displacement undergone before the lobe pattern repeats. So any four-lobed pipe will have twisted [1/4] turn or an angle of 90° in one increment of twist. Transition zones were of the shortest possible length (thereby the length for one increment of twist) to avoid unnecessary pressure loss. For a pipe of diameter 0.05 m and pitch-to-diameter ratio 8, this is 0.1 m.

Design of a Variable Cross-Section Duct

The transition consists of a gradual change from circular cross section to lobed cross section (Figure 2). Two main types of transition were defined, based on the relationship of lobe area growth with length along the pipe.

Cross-section development: α and β transitions

Two ratios, α and β, describe the development of the variable geometry in different ways. The α-transition is the simplest, describing the geometry at an intermediate position as a ratio of the area of the lobes at that position (A_{Li}) to the fully developed lobe area A_{Lfd}, i.e.

$$\alpha = \frac{A_{Li}}{A_{Lfd}} \tag{3}$$

The β-transition arises from previously validated CFD cases (particularly for four-lobed swirl pipe) in which two distinctive types of flow could be identified, namely core flow and lobe flow.[1] It was observed that, with the four-lobed pipe, the core flow consisted mainly of axial velocity, whereas the lobe flow consisted mainly of tangential velocity, as shown in Figure 3b. Additionally, the four-lobed pipe showed less instability than the three-lobed, and had more distinct "core" and "lobe" flow of axial and tangential velocities. Therefore, it was postulated that a definition of the transition in terms of lobe area growth to core area (circular area only) would provide better results for four-lobed transition. The validation of this concept would be one of the first tasks of the optimization effort.

Hence the β-transition is defined as follows:

$$\beta = \frac{\frac{A_{Li}}{\pi R^2 - A_{Li}}}{\frac{A_{Lfd}}{\pi R^2 - A_{Lfd}}} \tag{4}$$

Development of variable geometry along the pipe

The next task was to relate the transitional ratios to axial distance along the pipe. The simplest option would be to express area ratio as a linear function of length, i.e.

$$\alpha, \beta = \frac{x}{L}$$

This would create discontinuities at the start and end of the development, and it was decided to apply a sigmoidal curve instead, i.e.

$$\alpha, \beta = \left[\frac{1 - \cos\left[\pi \frac{x}{L}\right]}{2}\right] \tag{5}$$

[1]Note that at least part of the flow is describing a helical path and that the cross section for this part will be slightly greater than the area equivalent.

[2]Another way to compute the equivalent diameter would be to calculate the hydraulic diameter (4 × cross-sectional area/perimeter). This gives a smaller diameter than the value used.

[3]Since the pipe has four lobes, there are four helices around the surface of the pipe. This gives four positions within one pitch length, in which the cross section appears identical. The fourth defines a full pitch.

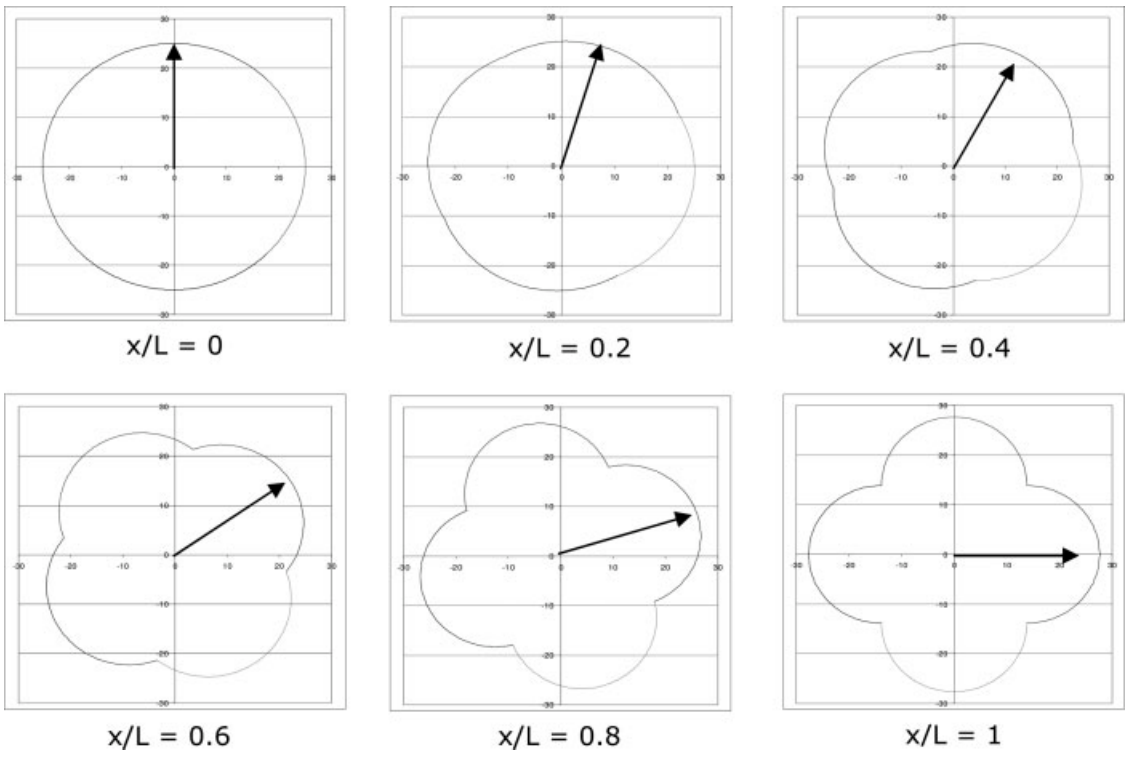

Figure 2. Transition development along pipe length; *x/L* represents length ratio.

The utilization of a cosine function avoids the discontinuity that would result from the use of a linear relationship, as illustrated by the linear law in Figure 4, giving a smooth transition.

Figure 4 shows the comparison of α and β transition and how the lobe area develops in each of these cases. Note that for β-transition the lobe development is faster than for α transition. It was expected that this would result in greater swirl induction in the β-transition since the lobes prevail for a longer length, and tangential velocity is concentrated in the lobe areas of the pipes.

The sigmoidal function given in Eq. 5 required a further optimization control to smoothen or sharpen its shape. This can be provided by redefining the lengthwise function, as described in the following section.

Transition exponent

As a further refinement, a transition exponent, n, was used to create a set of transition curves by the variation of its value, as shown in Figure 5.

Equation 5 is then changed to

$$\alpha, \beta = \left[\frac{1 - \cos\left[\pi \frac{x}{L}\right]}{2}\right]^n \tag{6}$$

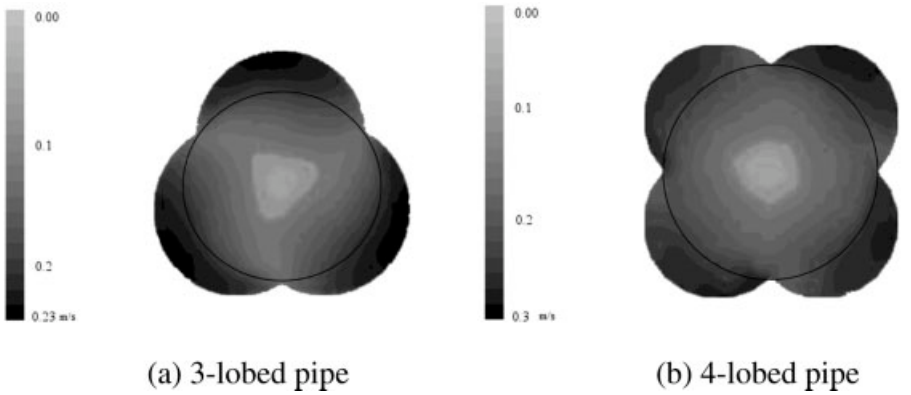

Figure 3. Tangential velocity contours at exit of swirl pipe.

(Circular outline indicates "core").[1] (a) Three-lobed pipe; (b) four-lobed pipe.

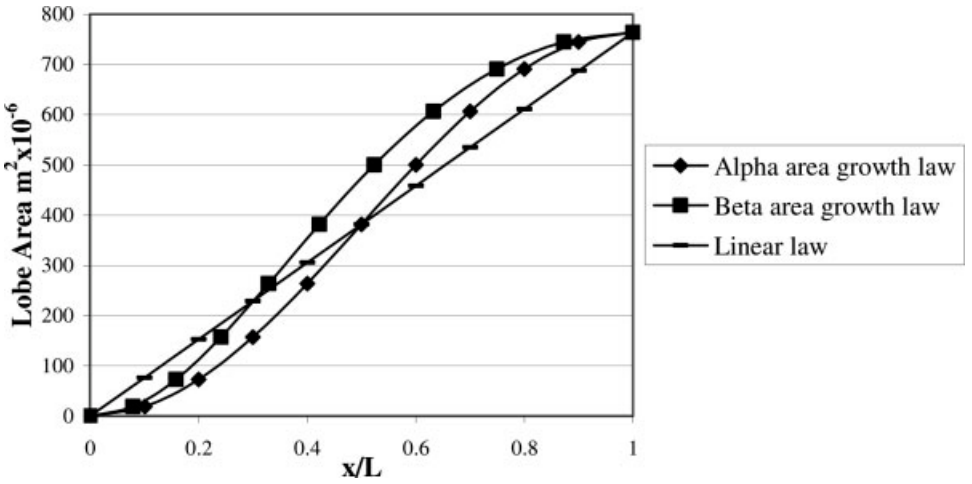

Figure 4. Entry transition; comparison of lobe area development with length for α and β and linear law.

Thus the transition exponent n is 1 for the simple transitions explained in previous paragraphs.

For α-transition when

- $n < 1$: the 50% point of lobe development is brought nearer the start,
- $n = 1$: the 50% lobe development point is at exactly midlength,
- $n > 1$: the 50% point is further away from the 50% length point.

In the case of β-transition, the 50% point of lobe development is nearer the start than for α-transition for each case of transition exponent n. This implies greater area growth at the front of the transition and, therefore, a quicker lobe development for β-transition.

CFD Methodology

As analysis was needed for a wide range of geometries, experimental testing would be costly and time-consuming. Computer modeling eliminates the difficulty and cost of making the pipes, and gives an insight into the flow field which is difficult to measure experimentally. Fluent v6.0 CFD software was used with its preprocessor Gambit for creating the swirl pipe geometry and meshing all geometries. The transition geometries were created using ProEngineer software.

The CFD predictions were single phase, consisting pure fluid (water) only. A starting solution or "baseline" was needed to make prototypes for physically testing more complex mixtures and rheologies, and whatever the proposed duty of the pipe, at some stage or other it will almost certainly be carrying only liquid. In cases where settling solids were present, a smooth mechanical action would carry them into the extant swirling flow. Solutions for more viscous liquids and slurries with finer particle burdens are a subject for continuing research.[15,16]

A set of assumptions were made to simplify the problem of flow within swirl pipes:

- The flow was assumed to be steady and isothermal.

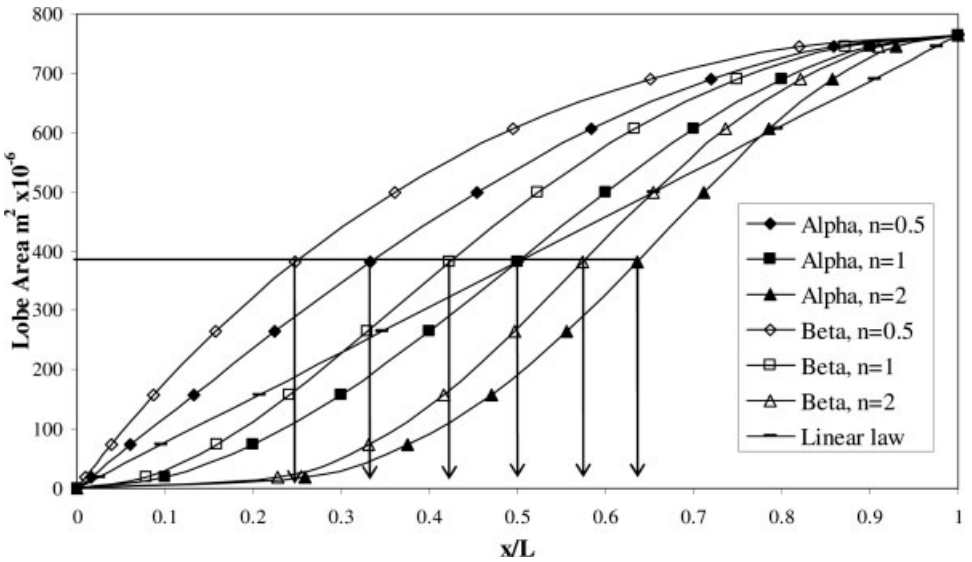

Figure 5. Entry transition: effect of transition exponent (arrows point to 50% lobe development point).

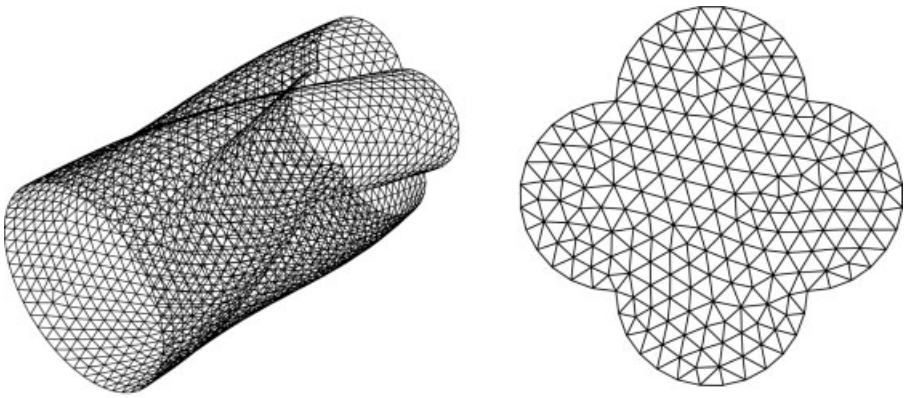

Figure 6. Typical four-lobe transition pipe hybrid mesh generated in Gambit.

(a) Isometric view; (b) cross-sectional view.

- Fully turbulent flow was assumed at the inlet of the pipe.
- The "no-slip" boundary condition was employed at the wall.
- The pressure drop was estimated by considering hydraulically smooth pipes, unless otherwise stated.
- Effects of molecular viscosity were assumed to be negligible in the fully turbulent region.

A tetrahedral/TGrid mesh was used for all swirl and transition geometries. This is an unstructured mesh where the cells are positioned in an irregular manner and gives greater flexibility for complex geometries such as swirl-inducing pipes, which can involve sharp angles, for example, at the intersection of the lobes. The mesh for a typical entry transition pipe is shown in Figure 6.

An inlet boundary condition of uniform mean flow velocity was used for entry transition simulations. In exit transition simulations, velocity profiles from the exit of an optimized constant geometry swirl pipe were used. An outlet boundary condition of zero uniform static pressure was specified in all cases.

The standard k-ε model of turbulence was used with standard wall functions. The standard k-ε turbulence model is primarily valid for fully turbulent flows. Standard wall functions were used to "bridge" the viscosity-affected region between the wall and the fully developed turbulent region. This approach uses the "log law," whereby the mean velocity is taken as a logarithmic function of the distance from the wall in the fully turbulent region. Therefore when using standard wall functions, the distance from the wall of adjacent cells must be determined, considering the distance over which the log-law is valid ($30 < y^+ < 60$).[1,17,18] Therefore, using an excessively fine mesh near the walls was avoided, because the wall functions cease to be valid in the viscous sublayer ($y^+ < 30$). Where necessary in the simulations, the near-wall mesh was refined to ensure that the wall-adjacent cells were located within the log-law layer ($y^+ < 60$).

Previous research[1,11] established that the standard k-ε model was sufficient for repetitive and time-consuming investigative trials involving swirl pipes. Although renormalization group k-ε (RNG), realizable k-ε model, or Reynolds stress model (RSM) should show substantial improvements where the flow features include streamline curvature and rotation,[17] the accuracy gained was not considerable when the extra time consumed was taken into account. The use of RSM turbulence model is recommended[17] when swirl intensity (see Eq. 1) is greater than 0.5. In the case of swirl and transition geometries, the swirl intensity does not generally exceed 0.2.

The flow parameters which were assumed for the simulations are summarized in Table 1.

To establish that the results of the simulations were largely independent of the mesh size, grid-independence tests were carried out for a single case of swirl, entry transition, exit transition, and cylindrical pipes. The initial grid in each case was refined by approximately doubling the number of elements. The values for pressure, average tangential velocity, swirl intensity, and swirl effectiveness (where applicable) were checked for convergence.

CFD Optimization of Transition Geometry

It was determined whether, as predicted, the β transition design was an improvement on the basic α transition design, and how transition pipes compared to optimized constant ge-

Table 1. Flow Parameters for the CFD Simulations

Parameter	Value
Length of pipe (transition/swirl/combination) (m)	0.1–0.6
Axial velocity (u) at inlet* (m s^{-1})	1.5
Radial velocity (v) at inlet* (m s^{-1})	0
Tangential velocity (w) at inlet* (m s^{-1})	0
Reynolds number	75,000
Pressure at outlet (Pa)	0
Turbulence intensity at inlet	4%
Hydraulic diameter (m)	0.05
Density of water (kg $m^{-3)}$	998.2
Viscosity of water (kg m^{-1} s^{-1})	0.001

*Except where a velocity profile was loaded at the inlet.

Table 2. Comparison of α and β Transition Pipes ($n = 1$) and an Optimized Swirl Pipe (All Four-Lobed)

	Swirl Pipe	α-Transition Pipe	β-Transition Pipe
Length (m)	0.4	0.1	0.1
Tangential velocity (m s^{-1})	0.284	0.11	0.12
Pressure drop (Pa)	426.52	119.42	125.05
Swirl intensity	0.137	0.061	0.068
Swirl effectiveness	0.36	0.58	0.61

ometry swirl pipes. Table 2 summarizes a comparison of simulation results for α and β entry transitions ($n = 1$, i.e. before application of transition exponent) and optimum swirl pipe. The results given are average values at the exit of the pipes.

The transition pipes were more efficient at swirl induction than the optimized constant geometry swirl pipe itself, since their swirl effectiveness value was greater. This is because the gradual transition from circular cross-sectional geometry to lobed geometry reduces frictional pressure losses from pipe walls, thereby producing a more efficient swirl. However, the overall tangential velocity produced by the transition pipe was not as high as constant geometry swirl pipe. Contour plots of tangential velocity (Figure 7) show the well-developed swirl at the exit of the optimized constant geometry swirl pipe in comparison to the developing swirl at the exit of the transition pipe. Therefore, the pipe should be considered in its entirety, with transitional geometry leading to constant or near-constant geometry and followed by exit transitional geometry.

As expected, β-transition was more effective at swirl induction than α, with a value of swirl effectiveness 5% greater than α. Therefore, further optimization was carried out on β-type transition only.

Optimization of transition exponent for entry transition

A uniform axial velocity of 1.5 m s^{-1} was used. Several β-transition geometries were produced for different values of transition exponent, n. These geometries were then meshed in accordance with grid independence results, and CFD simulations were carried out. The tangential velocity, pressure drop, and swirl effectiveness were calculated at the exit of the pipes and plotted against the transition exponent value of the relevant pipe (Figure 8).

The smaller the value of the transition exponent, n, the greater was the tangential velocity generated, however, the greater was the pressure loss. The swirl effectiveness parameter is a balance of these two values. The swirl effectiveness was maximum at a value of $n = 0.5$. This is a case where the lobes develop faster in the transition than with the initial β case of $n = 1$.

Optimization of transition exponent for exit transition

A velocity profile from the exit of an optimized constant geometry swirl pipe was used at the inlet to exit transition pipes, with geometry defined by varying values of transition exponent n.

The results at the exit of the transition were plotted (Figure 9). The same geometry as for entry transition, with exponent $n = 0.5$, showed maximum swirl effectiveness and, therefore, was optimum for the exit transition. This is a case where the lobe dissipation is slower at the start of the exit transition pipe, thereby sustaining the swirling lobe flows for longer than the initial case of β $n = 1$. Overall trends of tangential velocity and pressure drop with respect to transition exponent were similar to trends from entry transition.

Advantage from Transitions

CFD simulations were then carried out to establish the advantage from using entry and exit transition zones in conjunction with constant geometry swirl pipes in place of cylindrical pipes. Model parameters were as detailed earlier. The geometries used in the simulations were as illustrated in Figure 10. The results given are for a near-optimum transition case (β-transition $n = 1$). The flow direction was reversed for the exit transition case.

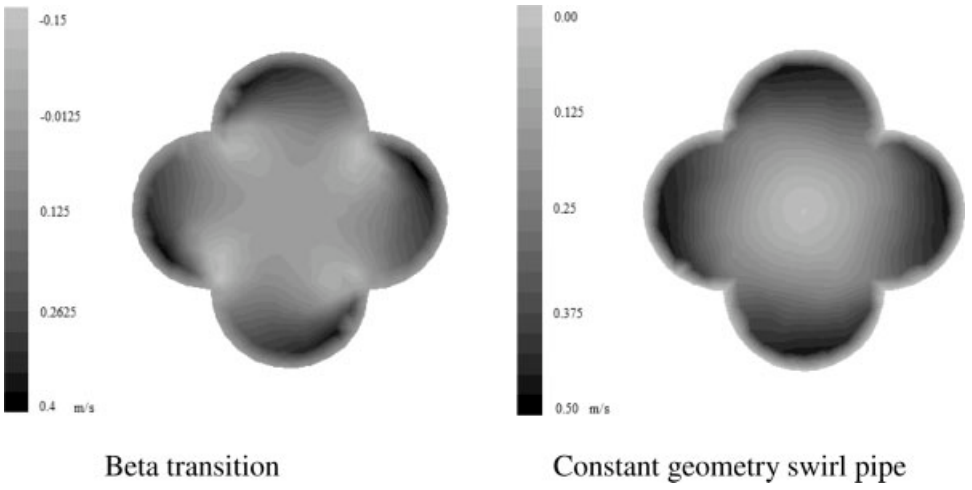

Figure 7. Contours of tangential velocity at the exit; transition length 0.1 m, swirl pipe length 0.4 m.
(a) β transition; (b) constant geometry swirl pipe.

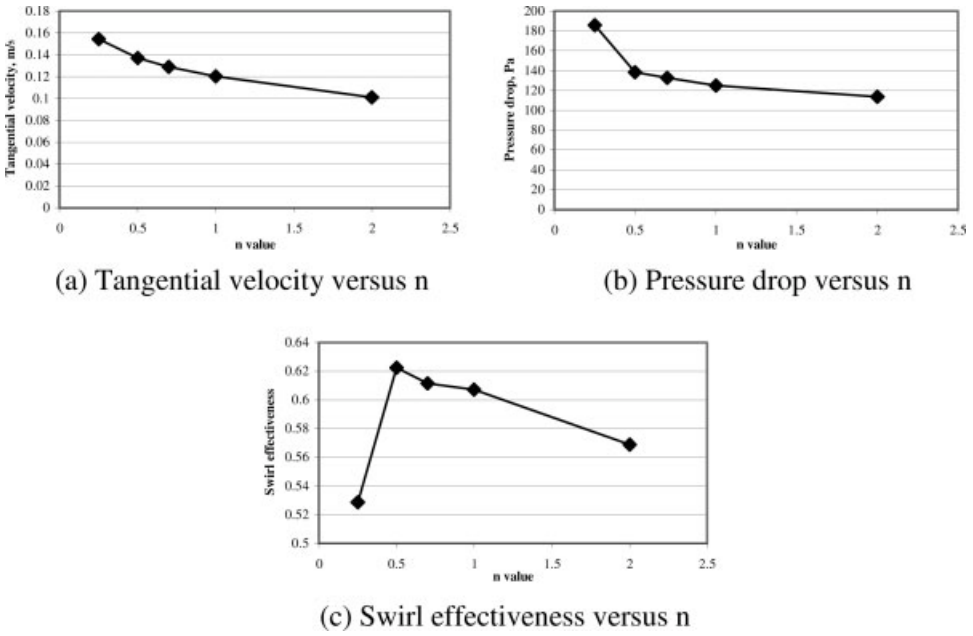

Figure 8. Entry transition optimization.

(a) Tangential velocity vs. *n*; (b) pressure drop versus *n*; (c) swirl effectiveness vs. *n*.

Entry transition

Where entry transition was used, initial pressure loss was greater due to the lobed geometry of the transition, as opposed to the smooth walls of the cylindrical pipe (Figure 11b). However, at the entrance to the constant geometry swirl section, there was a smooth transition of flow from one pipe to the next, and the pressure loss that resulted due to sudden change in cross section was avoided. Therefore, post-transition pressure loss remained substantially lower than with cylindrical pipe.

In addition, the transition generated an initial high tangential velocity, which continued inside the constant geometry swirl section (Figure 11a). With cylindrical pipe inlet, the tangential velocity was negligible until the entry point of the

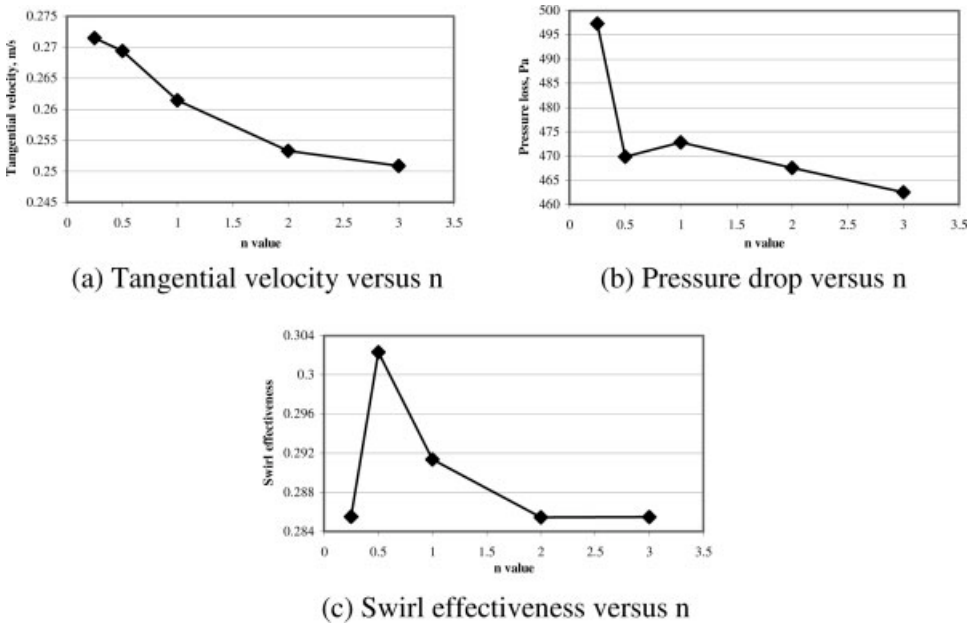

Figure 9. Exit transition optimization.

(a) Tangential velocity vs. *n*; (b) pressure drop vs. *n*; (c) swirl effectiveness vs. *n*.

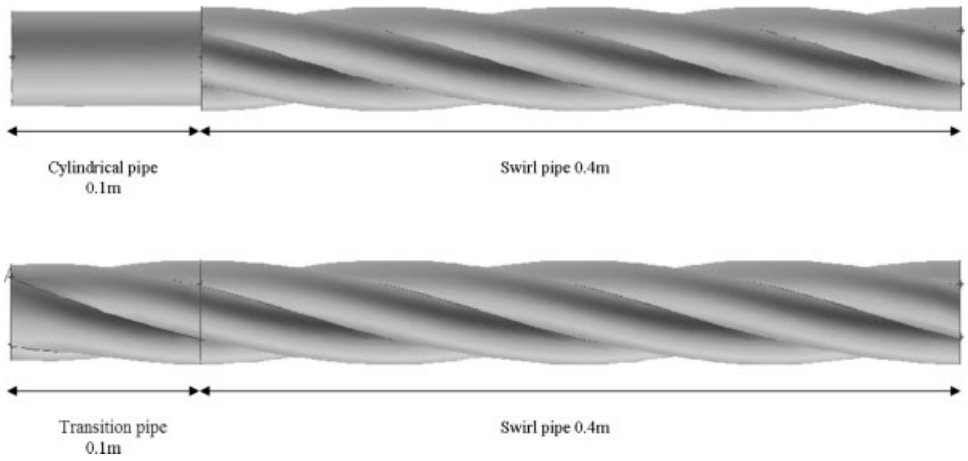

Figure 10. Simulation geometry for advantage of entry and exit transition as opposed to cylindrical pipe.

constant geometry swirl pipe (0.1 m length), where there was a high rate of tangential velocity generation. However, the tangential velocity generated remained lower than that with entry transition. The length of swirl pipe required to achieve a certain tangential velocity was less when the transition was incorporated at the start.

It is also evident from the negative slope in Figure 11c that the constant geometry swirl pipe was constraining the tangential velocity generated by the transition pipe. In future, it may be worth investigating, changing the pitch of the swirl pipe along its length, as attempted by Raylor and coworkers[3,4] to sustain the additional swirl generated by the entry transition. The overall effect of increased tangential velocity and reduced pressure loss was greater swirl effectiveness (Figure 11c).

Exit transition

The tangential velocity was almost equivalent in both cases of cylindrical exit pipe and exit transition (Figure 12a). However, Figure 12c shows that the inclusion of exit transition reduced the rate of decay of swirl. The half-life of swirl was increased from 15 to 20 diameters. Once again, exit pressure losses from sudden cross-sectional change were reduced (Figure 12b).

Experimental Validation of CFD Model

The main variables of importance in CFD simulations were pressure drop and tangential velocity, since these are the parameters that determine swirl effectiveness.

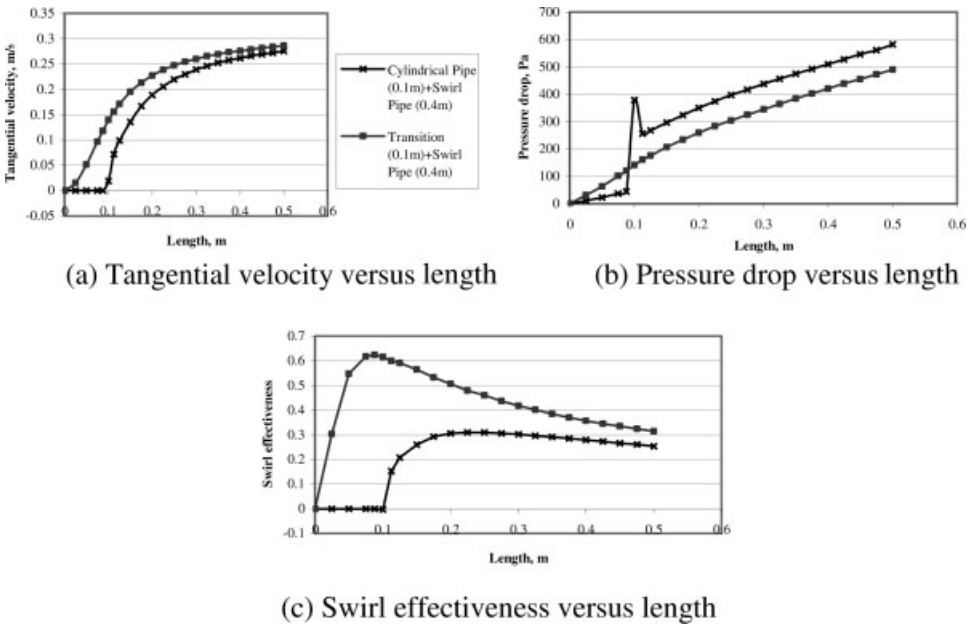

Figure 11. Comparison of use of entry transition to use of cylindrical pipe.

(a) Tangential velocity vs. length; (b) pressure drop vs. length; (c) swirl effectiveness vs. length.

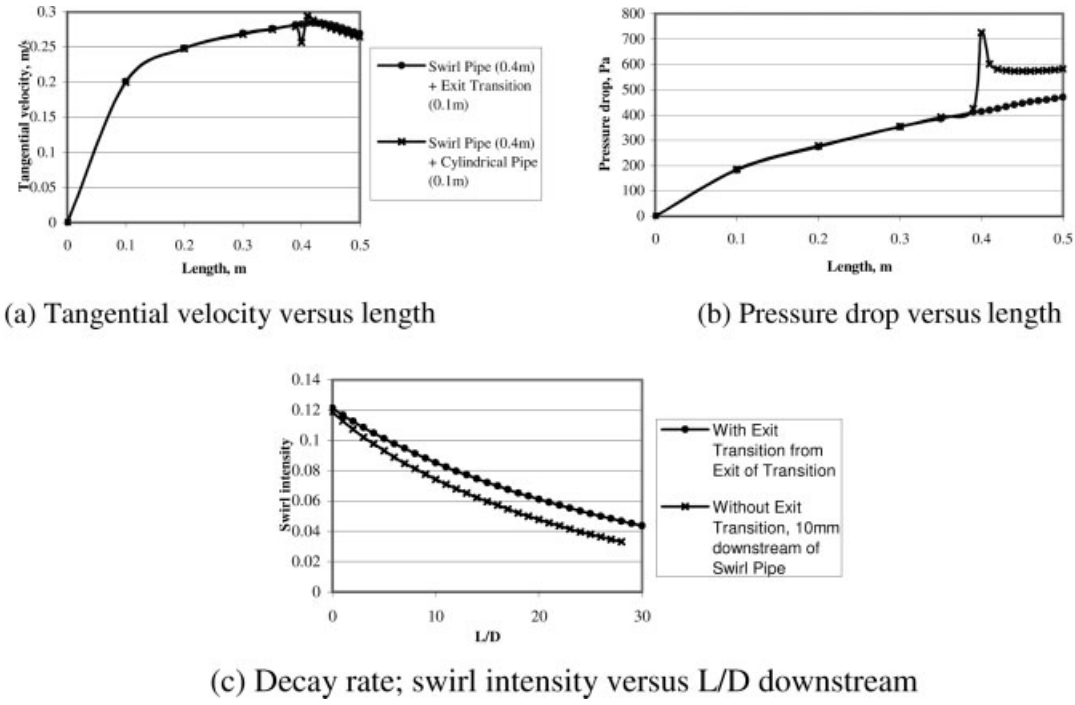

Figure 12. Comparison of use of exit transition to use of cylindrical pipe.

(a) Tangential velocity vs. length; (b) pressure drop vs. length; (c) decay rate; swirl effectiveness vs. *L/D* downstream.

Pressure drop

Pressure loss was measured on an experimental flow loop consisting of a horizontal section of 6.4 m length. Piezoresistive pressure transducers were used initially. However, due to rapid change in their calibration, measurements were repeated with an inverted manometer, which provided more accurate and reliable results. A 0.1 m four-lobed transition pipe ($\beta\ n = 0.5$, $P{:}D$ ratio $= 8$) was inserted on the flow loop in conjunction with an optimized 0.4 m constant geometry swirl pipe, and the pressure loss measured across a total pipe length of 3.33 m (which included 2.83 m of cylindrical pipe), avoiding bend effects.

It was necessary to measure the pressure at a substantial distance from the swirl-inducing pipes, because the swirling flow might otherwise have affected the results. All pressure tappings were therefore placed within cylindrical pipes and at a length of more than 1 m away from swirl-inducing pipes. The pressure drop due to additional cylindrical pipe was subtracted from the total experimentally measured value to obtain only the pressure loss across the swirl/transition

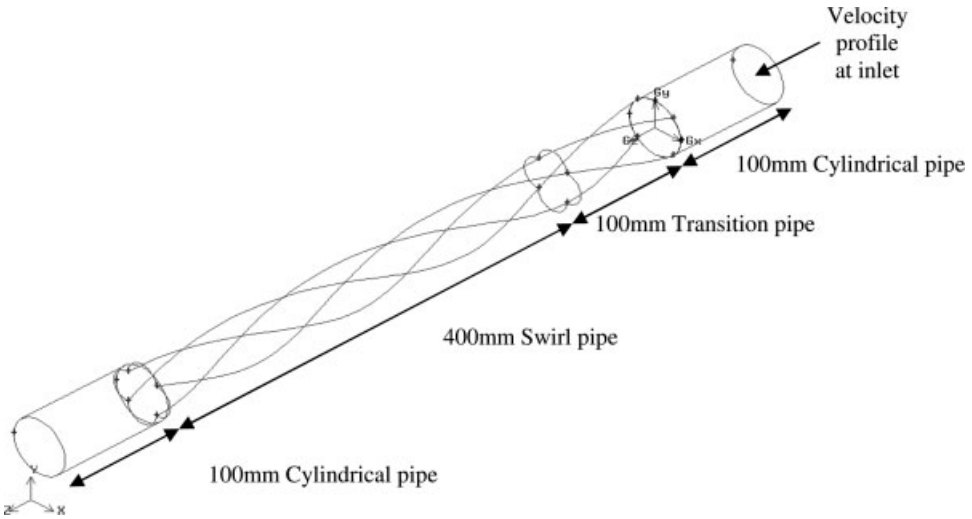

Figure 13. Geometry for CFD analysis of entry and swirl pipe pressure loss.

Table 3. Pressure Loss Results for Entry Transition and Swirl Pipe in Conjunction

Rig Velocity ($m\ s^{-1}$)	Experimental Pressure Drop (Pa)		CFD Pressure Drop (Pa)		Error, CFD RSM to Manometer (%)
	Manometer	Transducers	k-ε Model	RSM	
1.00	274.73	284.24	272.92	259.95	−5.68
1.22	391.30	407.89	417.18	398.04	1.69
1.49	535.00	526.99	591.19	564.43	5.21
1.73	705.82	776.34	791.57	753.47	6.32
1.97	903.75	935.66	1024.08	979.79	7.76
2.27	1128.81	1152.45	1284.33	1229.56	8.19

pipe geometry. The cylindrical pressure loss was approximated from previously determined experimental values.

The standard error in the manometer reading of pressure loss, taking into account errors due to subtracting cylindrical pipe pressure loss, was 2%–8.1%. The error was less than 2.2%, other than at the lowest velocity of 1 m s^{-1}.

The geometry used in the CFD simulation is illustrated in Figure 13. The pressure losses at the intersection of the cylindrical pipe and the swirl-inducing pipe are important for comparison with experiment. Therefore, sections of cylindrical pipe were added to the geometry at entry and exit. Surface roughness values of 2.09×10^{-06} m for the swirl and transition pipes, and 1.89×10^{-08} m for the cylindrical pipe were specified. These were experimentally measured roughness values for the Perspex cylindrical pipes and prototyped transition and swirl pipes used on the flow loop. The RSM of turbulence was used with an inlet velocity profile. Results from the use of standard k-ε turbulence model are shown for comparison. The pressure loss across entry transition and constant geometry swirl pipe only has been compared to the experimental value in Table 3 and Figure 14.

The maximum error between CFD prediction and experimental result was 8%. CFD tended to overpredict the pressure drop, with increasing velocity. Grid independence tests were carried out at a flow velocity of 1.5 m s^{-1}. Therefore, the grid may not have been sufficiently fine to resolve the greater turbulence generated at the higher velocities. Additionally, some preliminary studies indicated that the use of an unstructured tetrahedral mesh in place of a structured hexahedral mesh[19] may result in overprediction of pressure losses. Other possible explanations are the steeper velocity gradient near the wall at the higher velocities (introducing errors due to use of wall functions), the requirement of a longer length of cylindrical pipe length to establish a fully developed viscous boundary layer at the higher velocities, and the use of "uniform pressure" outlet boundary condition.

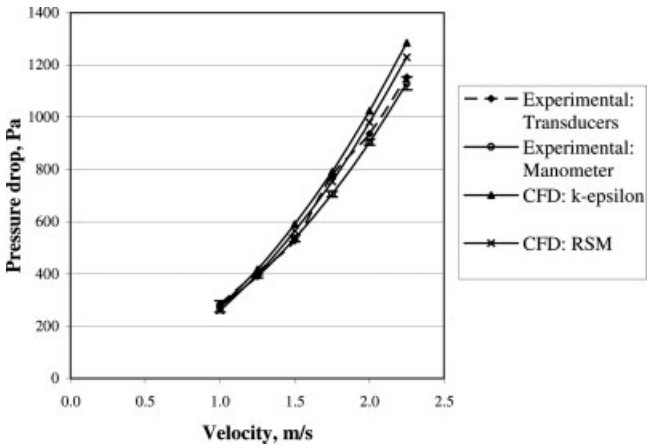

Figure 14. Pressure loss validation for a four-lobed entry transition pipe in conjunction with swirl pipe (standard error in manometer reading indicated on graph).

Tangential velocity

Particle image velocimetry (PIV) measurements of flow 0.25 m (L/D=5) downstream of an optimized constant geometry swirl pipe were obtained by Tonkin and coworkers[15,16] on a similar flow loop, as used for pressure loss measurements. Tangential velocity results have been extracted from these to validate CFD-predicted swirl.

The experimental results are shown in comparison with predicted results from CFD in Figures 15a–d, for varying axial flow velocities. An average tangential velocity at a given range of radial coordinate was calculated and plotted.

PIV indicated a maximum tangential velocity between $r/R = 0.7$ and 0.9. CFD predictions indicated a maximum at between 0.8 and 0.9. The error between PIV and CFD predicted values of maximum tangential velocity were within 20%. Overall, the points of least agreement between CFD and PIV were at the centre of the pipe and at the pipe wall. Some difference in the result from CFD and PIV may be owing to the discrepancy in axial velocity specified in the CFD simulation and the operating velocity of the flow loop (the lower maxima in Table 4 from CFD compared to PIV may be due to the lower axial velocity specified in CFD).

Conclusions

- Entry transition pipes are more efficient at swirl induction than constant geometry swirl pipes due to the gradual introduction of lobes, which reduces frictional pressure losses.
- Benefits from transition suggest that the pipe should be considered in its entirety with transitional geometry, leading to constant or near-constant geometry and followed by exit transitional geometry. In this way, new variations can be optimized for each zone of swirl induction, without compromising the compatibility or synergy of the whole.
- For the four-lobed transition geometry studied, a transition design based on ratio of lobe area growth to core area

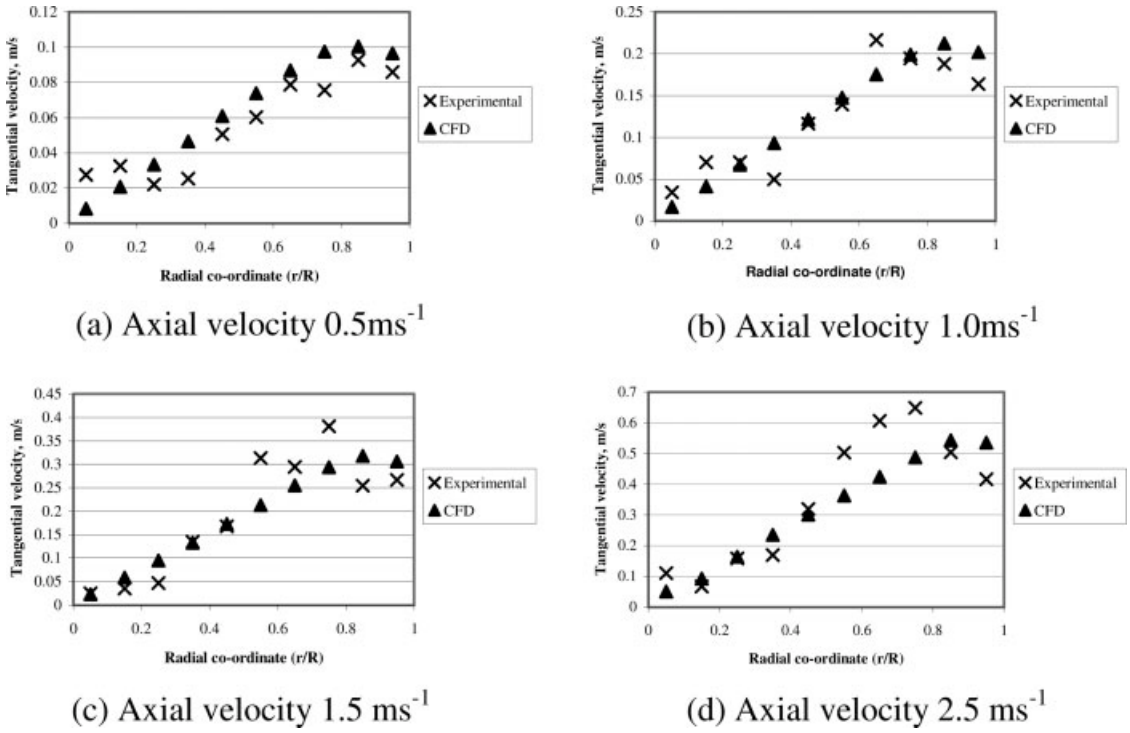

Figure 15. Comparison of experimentally measured tangential velocity to CFD prediction at different axial velocities.

(a) axial velocity 0.5 m s^{-1}; (b) axial velocity 1.0 m s^{-1}; (c) axial velocity 1.5 m s^{-1}; (d) axial velocity 2.5 m s^{-1}.

and with greater development at the start of the transition (β design) was better than a basic design based on lobe area growth (α design). An optimum entry and exit transition geometry was determined from different designs based on the lobe development within the pipe.

- Future optimization with respect to length, where transitions are incorporated within the swirl pipe must be carried out, particularly since a shorter length is required to achieve equivalent swirl intensity with the inclusion of entry transition.
- The use of entry and exit transition reduces entry and exit pressure losses caused due to the sudden cross-sectional change in swirl pipes.
- Entry transition increases the overall-generated swirl intensity, whilst exit transition reduces swirl decay.
- The constant geometry swirl pipe restricts the initial high swirl generated by entry transition because of its constraining constant pitch. It may be worth investigating a variable pitch for the swirl pipe to maximize the advantage of entry transition.

Table 4. Maximum tangential velocities

PIV Axial Velocity (m s^{-1})	CFD Axial Velocity (m s^{-1})	PIV Tangential Velocity (m s^{-1})	CFD Tangential Velocity (m s^{-1})
0.5	0.5	0.1	0.11
1.1	1.0	0.3	0.25
1.7	1.5	0.4	0.38
2.8	2.5	0.7	0.64

- CFD predicted results of pressure loss and tangential velocity in swirling pipe flow are in good agreement with experimentally measured values.

Notation

ΔP = pressure loss, Pa
ρ = density, kg m^{-3}
A_{Lfd} = total lobe area for fully developed lobes, m^2
A_{Li} = intermediate lobe area, m^2
D = pipe diameter, m
L = total pipe length, m
R = pipe radius, m
r = radial point at which parameters are evaluated, m
S = swirl intensity
u = axial velocity, m s^{-1}
w = tangential velocity, m s^{-1}
x = intermediate pipe length, m
y^+ = nondimensional distance of a point from the wall

Literature Cited

1. Ganeshalingam J. Swirl Induction for Improved Solid–Liquid Flow in Pipes. PhD Thesis, University of Nottingham, 2002.
2. Wood RJK, Jones TF, Miles NJ, Ganeshalingam J. Upstream swirl-induction for reduction of erosion damage from slurries in pipeline bends. *Wear*. 2001;250:770–778.
3. Raylor B. Pipe Design for Improved Distribution and Improved Wear. PhD Thesis, University of Nottingham, 1998.
4. Raylor B, Jones TF, Miles NJ. Helically formed pipes improve the efficient transportation of particle-laden liquids. In: Proceedings of the 14th International Conference on Hydrotransport, Maastricht, The Netherlands, September 8–10, 1999.

5. Wang M, Jones TF, Williams RA. Visualisation of asymmetric solids distribution in horizontal swirling flows using electrical resistance tomography. *Chem Eng Res Des*. 2003;81(A8):854–861.
6. Heywood NI, Alderman NJ. Developments in slurry pipeline technologies. *Chem Eng Prog*. 2003;99:36–43.
7. Wolfe SE. The transport of solids in helically-ribbed pipes. *CIM Bull*. 1967;60:221–223.
8. Schriek W, Smith LG, Haas DB, Husband WHW. The potential of helically-ribbed pipes for solids transport. *CIM Bull*. 1974;67:84–91.
9. Charles ME, Cheh CH-S, Chu LH-L. The flow of "settling" slurries in tubes with internal spiral ribs. *Can J Chem Eng*. 1971;49:737–741.
10. Singh VP, Charles ME. The flow of sand/water slurries in horizontal pipes with internal spiral ribs-effect of rib height. *Can J Chem Eng*. 1976;54:249–254.
11. Jones TF, Ganeshalingam J. Towards optimal swirl inducing pipe. In: Proceedings of the 15th International Symposium on Hydrotransport, Banff, Canada, June 3–5, 2002.
12. Steenbergen W, Voskamp J. The rate of decay of swirl in turbulent pipe flow. *Flow Measure Instrum*. 1998;9:67–78.
13. Li H, Tomita Y. Characteristics of swirling flow in a circular pipe. *J Fluids Eng*. 1994;116:370–373.
14. Jones TF, Ganeshalingam J, Raylor B. Duct with spiral groove. US Patent 10/512 286.
15. Jones TF, Tonkin RJJ. Velocity distributions in swirling pipe flows. In: Proceedings of the 16th International Conference on Hydrotransport, Santiago, Chile, April 26–28, 2004.
16. Tonkin RJJ. Swirling Pipeflow of Non-Newtonian and Particle-Laden Fluids. PhD Thesis, University of Nottingham, 2004.
17. Fluent Inc. Fluent 6.0 Documentation, User's Guide. Lebanon, NH: Fluent, 2001.
18. Launder BE, Spalding DB. The numerical computation of turbulent flows. *Comput Methods Appl Mech Eng*. 1974;3:269–289.
19. Ariyaratne C. Design and Optimisation of Swirl Pipes and Transition Geometries for Slurry Transport. PhD Thesis, University of Nottingham, 2005.

Manuscript received July 10, 2006, and revision received Dec. 21, 2006.